INDERSCIENCE PUBLISHERS
Linking academia, business and industry through research

International Journal of Surface Science and Engineering

ISSN online: 1749-7868 - ISSN print: 1749-785X
https://www.inderscience.com/ijsurfse

Enhancing tribological and corrosion performance of SLM fabricated AlSi12Mg components through ultrasonic assisted magnetic abrasive finishing

Maraboina Raju, Pasam Vamsi Krishna

DOI: 10.1504/IJSURFSE.2024.10066299

Article History:

Received:	23 September 2023
Last revised:	06 November 2023
Accepted:	18 November 2023
Published online:	04 March 2025

Enhancing tribological and corrosion performance of SLM fabricated AlSi12Mg components through ultrasonic assisted magnetic abrasive finishing

Maraboina Raju* and Pasam Vamsi Krishna

Department of Mechanical Engineering,
National Institute of Technology Warangal,
Warangal, Telangana, 506004, India
Email: maraboinaraju1992@gmail.com
Email: vamsikrishna@nitw.ac.in
*Corresponding author

Abstract: Selective laser melting (SLM) is one of the most important additive manufacturing (AM) techniques, which produces complex parts through layer-by-layer fabrication. However, some crucial issues such as poor surface quality and lack of dimensional accuracy that directly affect wear resistance, hardness, and corrosion properties, must be addressed before SLM parts can be widely used in real-time applications. Ultrasonic assisted magnetic abrasive finishing (UAMAF) is a hybrid finishing process that combines ultrasonic vibrations with traditional magnetic abrasive finishing (MAF) processes to process surfaces up to nanometre scale in the least possible time. This paper focuses on developing UAMAF framework and finishing SLM-produced parts made of AlSi12Mg alloy with unbonded silicon carbide abrasives. EDAX analysis showed no change in elemental composition when UAMAF combined with grinding was employed and the drop in hardness was 6.34% and 24.94% in non-heat-treated and heat-treated samples, respectively. Wear tests conducted on these samples revealed that the heat-treated ground-finished samples were less prone to the total wear. Corrosion tests conducted on the samples showed UAMAF reduced corrosion rate which is 95.69% and 91.35% in heat-treated and non-heat-treated samples, respectively.

Keywords: UAMAF; selective laser melting; SLM; micro hardness; wear analysis; corrosion analysis; SiC abrasives; magnetic abrasive finishing; MAF.

Reference to this paper should be made as follows: Raju, M. and Krishna, P.V. (2025) 'Enhancing tribological and corrosion performance of SLM fabricated AlSi12Mg components through ultrasonic assisted magnetic abrasive finishing', *Int. J. Surface Science and Engineering*, Vol. 19, No. 1, pp.22–42.

Biographical notes: Maraboina Raju is a PhD student at the Department of Mechanical Engineering, National Institute of Technology Warangal, India. He is having one year of experience in teaching and research. His research interests are ultrasonic assisted magnetic abrasive finishing, abrasive flow machining, additive manufacturing, unconventional machining. He published one research paper in reputed journals.

Pasam Vamsi Krishna is currently working as a Professor in the Department of Mechanical Engineering, National Institute of Technology Warangal, India. He is having 20 years of experience in teaching and research. His research interests are application of solid lubricants in machining process, application of eco-friendly nano cutting fluids in machining, vibration assisted machining,

modelling and simulation of manufacturing processes and composite materials. He has an active research group of PhD scholars and PG students. He completed four funded projects and two are ongoing. He published one text book, two text book chapters and edited three books. He published more than 125 research papers in reputed journals and conferences. He is an editorial board member for ten journals and delivered 30 guest lectures.

1 Introduction

In recent times, additive manufacturing (AM) has been playing a significant role in the manufacturing sector due to its flexibility in manufacturing geometrically complex parts, negligible material wastage, and increased productivity (Wong and Hernandez, 2012). Metal AM techniques are predominantly divided into powder feed, powder bed, and wire feed systems. Each technique has its own advantages and limitations. Selective laser melting (SLM) belongs to a powder bed system in which powder of the desired layer thickness is first spread on a build plate using a roller and then laser scans the desired area until the entire part is built (Frazier, 2014). The main advantage of powder bed techniques like SLM over others is its ability to produce high-resolution parts, retain complex internal passages, and maintain dimensionality (Spears and Gold, 2016). A great deal of work has been done on the manufacturing of Al components using SLM technique and most of the research has focused on the strength, and microstructural analysis of AlSi10Mg (Singhal et al., 2023). High-end applications such as fabrication of aerospace components through SLM process demand superior surface quality. Partial bonding, unbound powder particles of the build material on the surface of the component due to variable thermal gradients and different curing timings make surface quality of SLM parts unsuitable for direct usage (Majeed et al., 2019). The possible defects in SLM parts are lack of fusion, gas pores, and impurities that affect the reliability of SLM fabricated parts. The lack of fusion is caused by improper process parameter selection that results in improper melt pool overlapping. Gas pores are caused by incomplete escape of gases from the melt pool while impurities are added during raw material processing. These defects result in the poor surface quality of SLM parts which in turn affect the fatigue life of component, dimensional accuracy, aesthetic appearance, etc. Post processing procedures like finishing, which improves surface texture and quality of the SLM parts is necessary on AM components fabricated through SLM process (Shiyas and Ramanujam, 2021).

Advanced finishing processes like MAF have significant influence on the improvement of surface quality. There is less possibility of microcracks on the workpiece surface while using MAF compared to traditional finishing techniques like grinding, honing, or lapping. The primary cause for this is the magnetic field, which controls and produces cutting force. Abrasive particles which are generally non-magnetic in nature are mixed with ferromagnetic particles like iron powder. The magnetic field generated by electromagnet align these ferromagnetic particles in the lines of magnetic field and these abrasive particles are entrapped between magnetic lines to form a flexible magnetic abrasive brush (FMAB) (Figure 1). Rotational speed given to the electromagnet make abrasive particles move randomly and impact the surface thereby processing the surface by micro-cutting and nano scratching and produce nanometre scale surface quality

(Yamaguchi et al., 2012; Yousefzadeh and Safari, 2012). Due to flexibility in finishing the complex geometries and internal surfaces efficiently, MAF has been widely used by most of the manufacturing sectors (Zhang et al., 2019). Research studies on the finishing ability of MAF have expanded rapidly. Zhu et al. (2022) investigated MAF of AM samples with different forming angles and their study revealed that MAF productively reduced high surface roughness of 4–10 μm (initially) to about 100 nm by effectively removing staircase effect, balling effect, and other defects. Wu and Yamaguchi (2018) performed MAF on SLM built 316L stainless steel components. The initial surface roughness of 60 to 100 μm produced in SLM process was bought down to 0.3 μm while it was over 1 μm in conventional abrasive finishing process. Cui et al. (2022) investigated the surface quality enhancement of SLM built curved surface made of AlSi10Mg alloy. The study revealed that due to unequal powder spreading on the build plate, unstable laser density and laser power during forming, there were unmelted, and over melted AlSi10Mg powder in the molten pool of sample. It was also found that ultrasonic cleaning of sample resulted in cavities at the unmelted areas and over melted areas which led to hemispherical protrusions. As a result of these defects, initial surface roughness of the sample was 2.12 μm; after MAF, the surface roughness reduced to 0.279 μm.

Ultrasonic assisted magnetic abrasive finishing (UAMAF) is an integration of ultrasonic vibrations to traditional MAF process in order to achieve the desired surface finish in less time (Figure 1) (Dixit et al., 2019). In MAF, abrasive particles trapped between the iron particles aligned along the magnetic force lines move with high velocity, impact surface and separate surface peaks from sample material because of which finishing takes place (Singh et al., 2006; Anjaneyulu et al., 2023). UAMAF is an improvised version of MAF in which extra velocity is given to abrasive particles by giving ultrasonic vibrations to the workpiece (Figure 1). Ultrasonic vibrations modify the path of abrasive particles to sinusoidal motion from linear and helical path showing the effect of ultrasonic vibrations. In UAMAF, the extra velocity made abrasive particles hit the surface a number of times and also with higher cutting force than in MAF, thus removing surface asperities in a shorter time compared to traditional MAF (Misra et al., 2019; Anjaneyulu and Venkatesh, 2023). Till date, most of the research has been carried out on MAF of cast parts, while MAF of AM components was found to be very rare and UAMAF of AM components is hardly found in the literature. Studies related to AM parts made of Al alloy AlSi10Mg is well established in literature but AlSi12Mg is a recently developed alloy in AM technology, which possesses superior properties in comparison with AlSi10Mg (Table 1). The superior heat conductivity and reduced density of AlSi12Mg make it a popular material for use in the production of engine components, particularly cylinder heads and engine blocks (Javidani and Larouche, 2014). Because the thermal diffusivity of Al-Si alloys decreases with increasing Si concentration, these materials have shown to be the most effective thermal storage materials for medium to high temperature storage applications (Tawalbeh et al., 2023). Housings, ducting, and manufacturing equipment are the widely used products of this alloy. In the automobile and aerospace industries also the utilisation is more (Raju and Hithaish, 2014). Hence, there is a need to explore its applicability in various fields and to study the finishing ability of UAMAF on the SLM fabricated AlSi12Mg components.

Figure 1 Concept of finishing in UAMAF (see online version for colours)

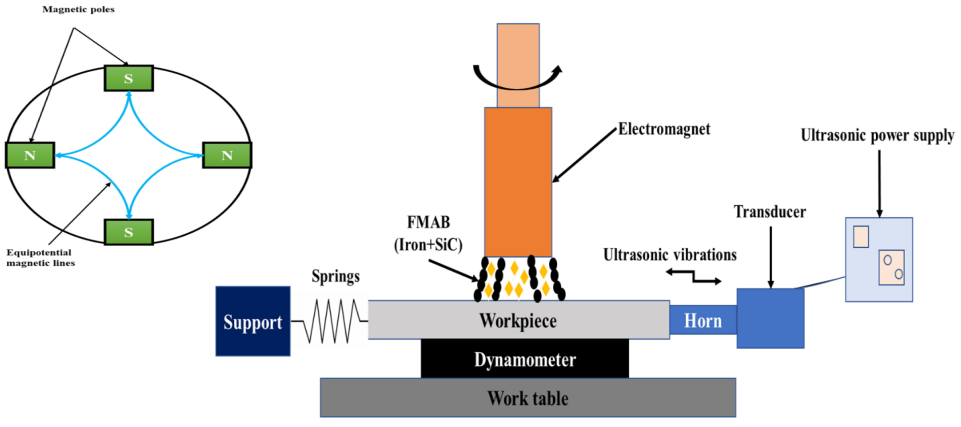

In the current work, experimental investigations related to UAMAF of SLM built samples made up of AlSi12Mg were carried out at constant machining parameters. The influence of heat treatment on the finishing ability of UAMAF was found in this study by building samples of heat treated and non-heat-treated type. To understand the significance of initial surface roughness on the finishing efficiency of UAMAF as-built samples and ground samples are used separately. To remove material in minute amounts, a grinding operation is utilised with a low feed rate and shallow cut depth. This is because conventional abrasive finishing processes result in abrasive embedment in to the workpiece surface. Abrasive embedment causes increase in hardness of AM parts which reduces efficiency of UAMAF process. After finishing the samples with UAMAF, comparative analysis was made between as built and ground samples in terms of microhardness, wear, and corrosion. EDAX analysis was performed to confirm elemental composition in various samples.

2 Materials and methods

Initially, samples were fabricated using SLM printer DMP flex 100, specifications of which are shown in Table 1. AlSi12Mg powder was used to build samples whose composition and mechanical properties are shown in Table 1. To decrease the cost of experimental work and considering specifications of SLM machine, sample size was fixed at 40 × 20 × 5 mm. UAMAF setup was developed on a vertical milling machine in which an electromagnet was placed at spindle position shown in Figure 3 and whose specifications are presented in Table 1. The material used in fabricating electromagnet is Mild steel with copper windings of 700 turns and the magnetic flux density generated was 1 to 1.5 Tesla. It is a DC device with two slip rings for continuous power supply. The maximum voltage of 30–50 V was used to avoid the burning of copper windings, which was observed from trail experiments. The electromagnet was fixed at spindle position to provide rotation upon which cutting velocity was given to abrasive mixture for the finishing sample. With the help of dimmerstat, voltage was varied and this in turn varied magnetic flux intensity which influences the rigidity of FMAB. The increase in rigidity of FMAB causes abrasive particles not to escape from FMAB thus increasing UAMAF

finishing efficiency. To connect DC power supply to the electromagnet, a rectifier was used to convert current from AC to DC. Carbon brushes with spring attachment were used for continuous contact while rotating, thus providing power to electromagnet during rotation for maintaining FMAB till the end of finishing operation [Figure 2(a)]. Silicon carbide abrasive powder mixed with iron particles (which forms FMAB) was used as cutting tool. The SiC abrasives are stable and chemically non-reactive, however after certain finishing time new cutting edges may develop due to its fragile nature. This may help to increase material removal rate and surface roughness, in turn reduces finishing time. Hence, the finishing time of ten minutes was selected in the present study based on trial experiments. On supplying voltage to electromagnet, ferromagnetic iron particles line up along the field of magnetic lines and abrasive particles were trapped between the magnetic lines to form FMAB, as shown in Figure 2(a). Micro-cutting and nano scratching were the mechanisms involved in material removal in UAMAF (Jayswal et al., 2005). The stress relieving was done by holding at 300°C for two hours in a heating furnace and then cooled. It is required to refine the grains and improve the mechanical properties. In addition to making a metal softer and ductile, heat treatment may also help to improve the strength, hardness, and impact resistant (Suniya and Verma, 2023).

Figure 2 Elements of UAMAF, (a) FMAB formed (b) primary and secondary fixture (c) sample inside secondary fixture (d) ultrasonic horn (see online version for colours)

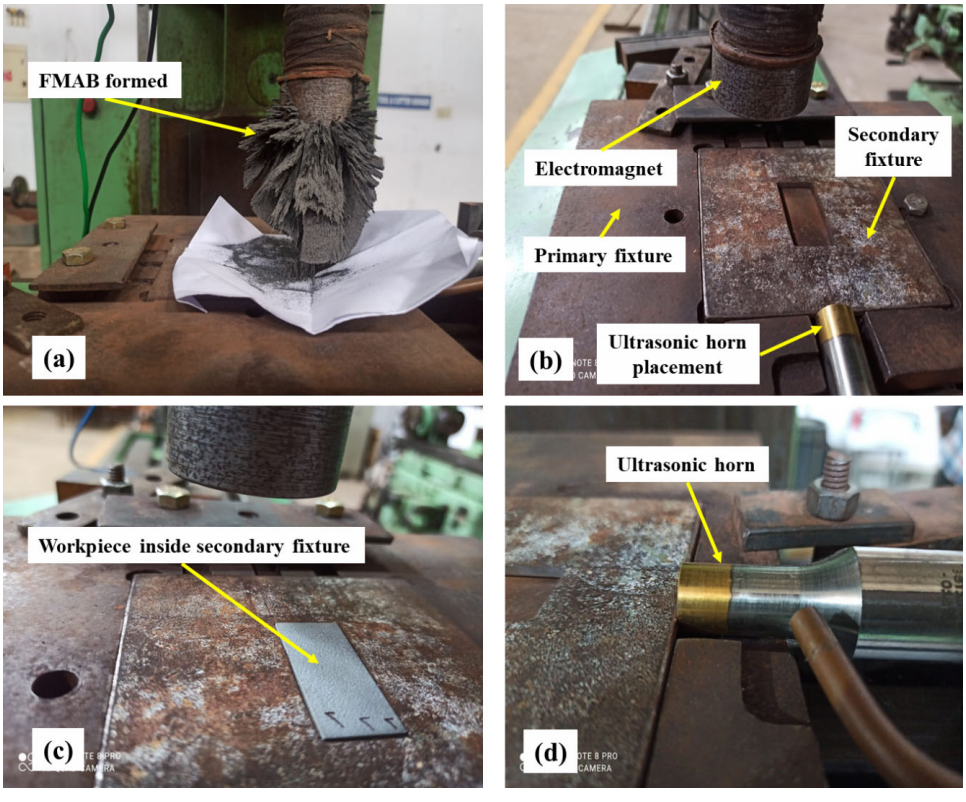

Table 1 Specifications and parameters in experiment

SLM machine specifications	
Power (W)	100
Scan speed (m/s)	1,000
Layer thickness (microns)	30
Hatch spacing (microns)	70
Build parameters	
Laser power (W)	300–380
Scan speed (mm/s)	2,500–3,500
Hatch distance (mm)	0.1–0.9
Stress relieving (HT)	300°C for two hours
Composition of sample	
AlSi12Mg: Al (59.30%), Si (< 4.26%), Mg (< 0.41%), O (< 13.52%), C (< 17.66%), Cu (< 0.58%), Zn (< 0.52%), Zr (< 3.34%)	
Mechanical properties AlSi12Mg alloy	
Elastic modulus (MPa)	76,600
Ultimate tensile strength (MPa)	153
Hardness (HV)	110
Density (kg/m^3)	2,684.95
Elongation at break (%)	0.5
UAMAF machining parameters	
Supplied voltage to electromagnet (V)	40
Rotational speed of electromagnet (rpm)	1,400
Ultrasonic frequency (KHz)	20
Abrasive weight (%)	25
Working gap (mm)	0.5
Iron mesh size (mesh no)	300
SiC mesh size (grit size)	180
Grinding process parameters	
Wheel speed (m/min)	1,100
Wheel grade	Very fine
Depth of cut (mm)	0.5
Wheel material	SiC
Feed rate (mm/rev)	5
Specifications of the electromagnet	
Electromagnet length (mm)	210
Length of copper winding (mm)	120
Gauge	26 wires
No. of turns	700 approximately
Magnetic flux density range	1 to 1.5 Tesla
Voltage range (V)	30–50

Figure 3 UAMAF experimental setup (see online version for colours)

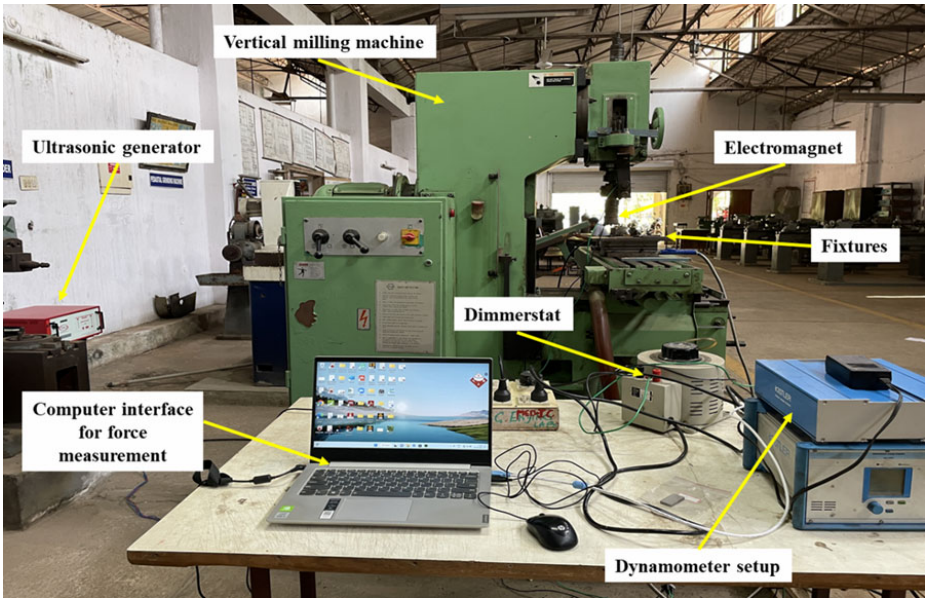

A special type of fixture (primary fixture) made of mild steel to hold the workpiece was fabricated and kept on work table of vertical milling machine [Figure 2(b)]. Primary fixture accommodates three springs and horn to supply ultrasonic vibrations to the workpiece. To place the workpiece, secondary fixture was fabricated and placed into primary fixture [Figures 2(b) and 2(c)]. The major objective of the secondary fixture is to accommodate workpieces that have smaller dimensions than the primary fixture, and the workpiece is created to that size to minimise the cost of sample manufacturing.

Table 2 Specifications of pin-on-disc apparatus

Parameter	*Range*
Sliding speed range	0.26–10 m/sec
Disc rotation speed	100–2,000 rpm
Maximum normal load	200 N
Frictional force	0–200 N
Wear measurement range	4 mm
Pin size	3–12 mm diagonal/diameter
Disc size	60 mm diameter × 8 mm thick
Wear track diameter	0–140 mm

Micro hardness was measured using Mitutoyo hardness testing machine with a measuring microscope of 0.1μ resolution and load range of 10 gf to 1,000 gf and testing was carried out according to ASTM E92:2017 standard. Wear tests were carried out on Pin-on-disc apparatus with fixed input parameters (Load 10 N, Sliding speed of 1 m/s, distance of 100 m) as shown in Table 2. The pin-on-disc experimental setup consisted of a rotating disc plate on which sample was placed. An input device was present to supply input

parameters to the rotating disc. A computer interface was present to collect data related to coefficient of friction.

Potentiodynamic polarisation testing method with three-electrode configuration was used for corrosion testing with parameters shown in table 3. AlSi12Mg was the working electrode, platinum wire was used as counter electrode and saturated calomel reference electrode (SCE) was used to quantify sample corrosion. Corrosion experiments were conducted according to ASTM G3-74 standard at ambient temperature and in an aerated 3.5% NaCl solution. PhadkeSTAT 20 Potentiostat was used for electrochemical investigation and the area exposed for testing was 1 cm^2 out of 2 cm^2 sample size, while the remaining area of sample was concealed with epoxy resin. Polarisation scan obtained by Potentiostat was used to predict corrosion properties of a test sample.

Table 3 Parameters for polarisation tests

Specification	*Value*
Scan rate (mV/s)	1
Sample period (s)	1
Stability (mV/s)	0.1
Open circuit delay (OCD) (s)	300

Applying potential of around ±250 Mv with open circuit potential led to the creation of polarisation curves, where anodic and cathodic branches were found in Tafel plots. Corrosion rate (CR) in mils per year (mpy) was calculated using equation (1) (Kottuparambil et al., 2018):

$$CR = \frac{Z_1 * i_{corr} * EW}{\rho} \tag{1}$$

where i_{corr} is corrosion current density in μA/cm^2, EW is equivalent weight of alloy, and ρ is density of alloy in gm/cm^2. Constant Z_1 is 3.27×10^{-3} mm g $(\mu A)^{-1}$ cm^{-1} $year^{-1}$. Here, i_{corr} was taken from Tafel plots, EW was taken to be 9 g and ρ was calculated according to Archimedes principle, and found to be 2.68 gm/cm^3.

3 Results and discussion

3.1 EDAX and micro hardness

Figures 4(a) and 4(b) shows EDAX analysis on the surface of Heat treated unfinished and non-heat-treated unfinished (As-built) sample. EDAX analysis on the samples revealed that Al is the parent material with Si, Mg as major alloying elements. Heat treatment of As-built sample showed negligible effect on the elemental composition of sample surface as shown in Figure 4(a). EDAX performed on samples that underwent grinding combined with UAMAF revealed that final finished sample showed no influence on elemental composition [Figures 4(c) and 4(d)]. Comparatively, oxygen present on non-heat-treated finished sample surface was more due to more oxide layer initially. Increased magnitude of cutting forces (Figure 5) by linear vibrations helped in removing oxide layer due to an increase in rapid abrasive moments thus decreasing oxygen in the case of finished sample, thereby increasing Al exposure. Low cutting forces are produced due to loosely

bound abrasives that shear off the material by rubbing action in UAMAF process. Active abrasive particles continuously strike the workpiece with very little force, since most of them are rolling on the workpiece and absence of stiff tool in touch with workpiece.

Figure 4 EDAX of sample surface, (a) HTR, (b) NHTR, (c) HT-GF, (d) NHT-GF (see online version for colours)

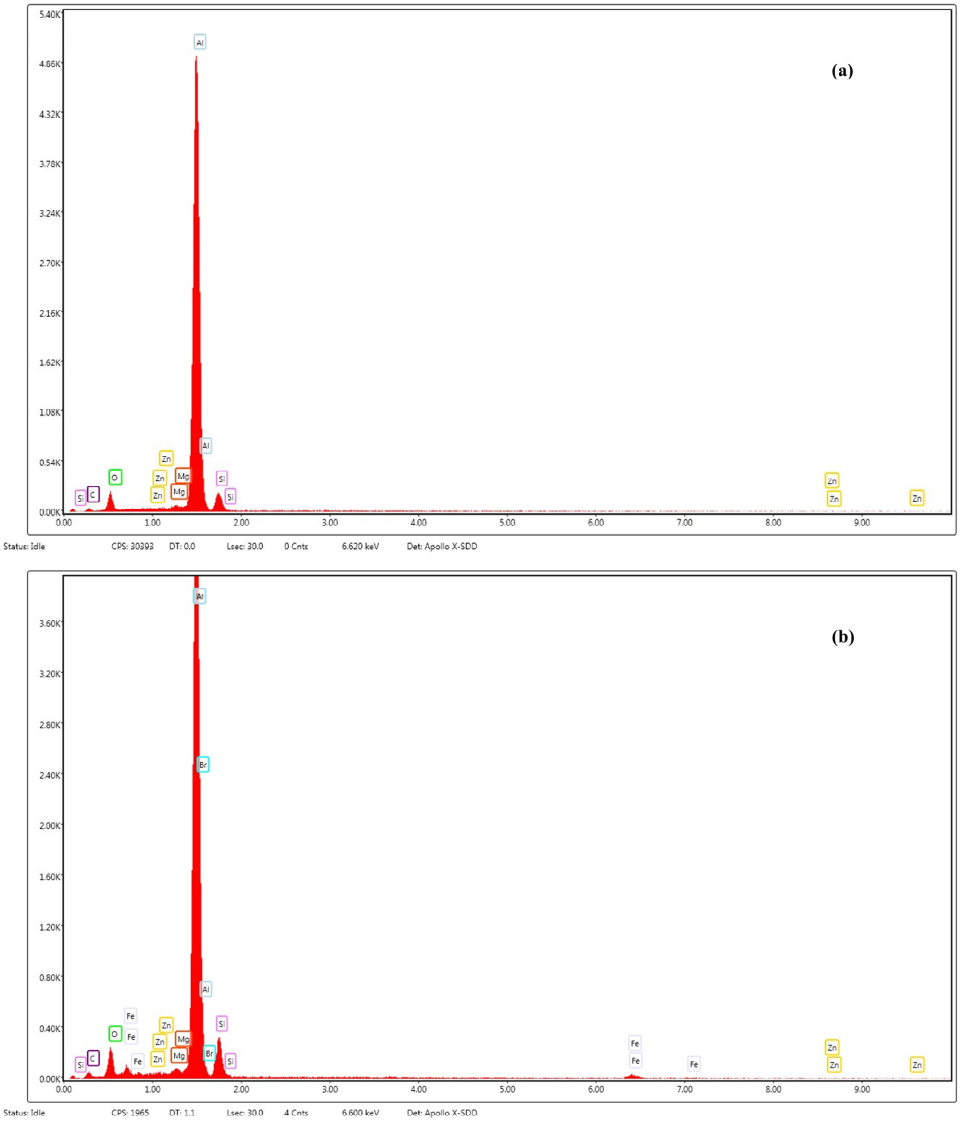

Figure 4 EDAX of sample surface, (a) HTR, (b) NHTR, (c) HT-GF, (d) NHT-GF (continued) (see online version for colours)

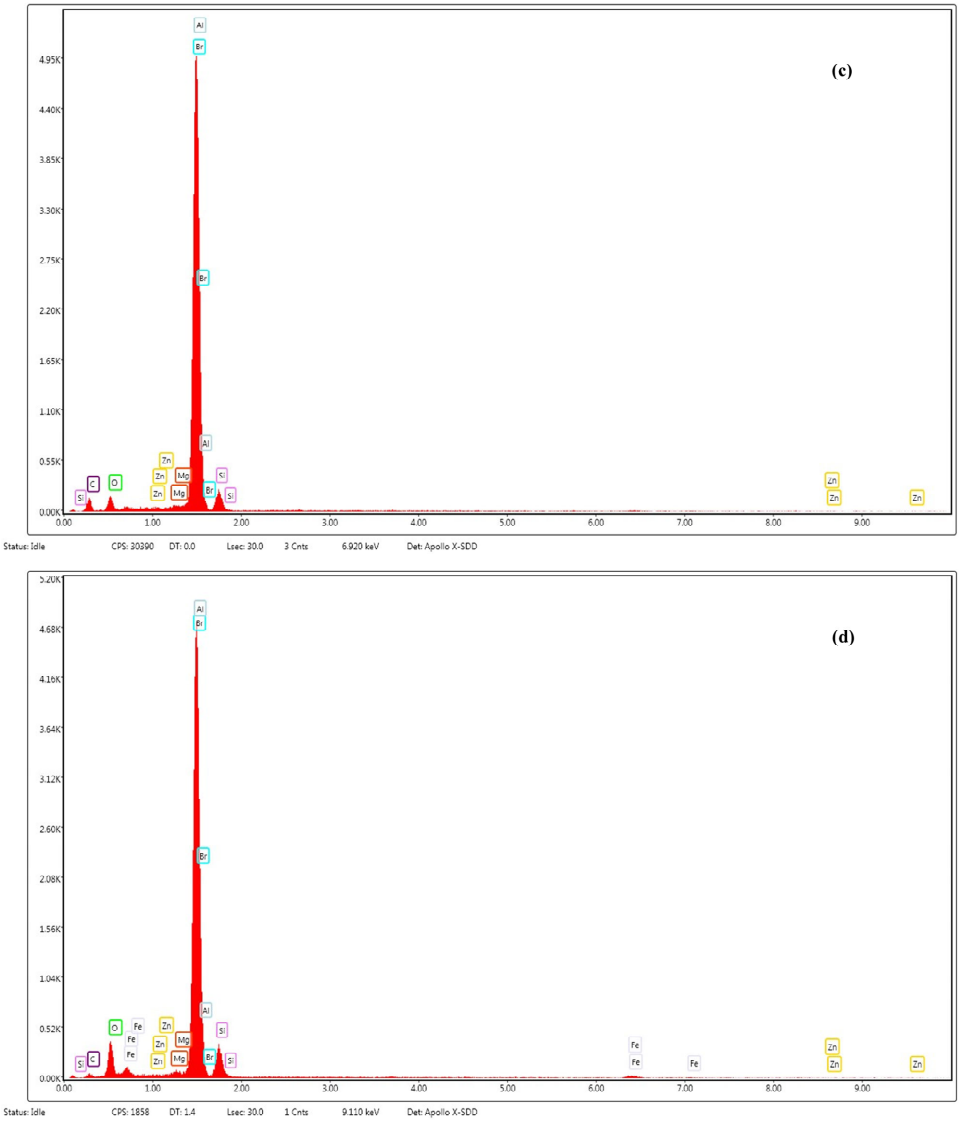

Figure 6 represents hardness of various sample types; the hardness of non-heat-treated unfinished sample was high due to rapid cooling rate which enabled the formation of fine grains and the fine grain formation led to increased grain boundaries (Aboulkhair et al., 2019). The hardness of the sample increased due to more strength being required in breaking the grain boundaries. Indentation depth, which is an indicator of hardness was more for heat treated sample compared to non-heat-treated sample. Heat treatment relieved surface hardening due to phase change from hard and brittle eutectic phase to coarse and ductile microstructure (Zhang et al., 2022). Hardness of heat-treated unfinished sample was lower compared to non-heat-treated unfinished sample because

heat treatment enabled grain refinement (Gite and Wakchaure, 2023). Hardness dropped after heat treatment due to the softening of material caused from grain coarsening and Si precipitating in Al-matrix. Hardness decreased after heat treatment due to an increase in the size of Si precipitate making precipitation and dislocation interactions differ. When the precipitate size was small in non-heat-treated unfinished samples, there was obstruction to dislocation by Orowan looping mechanism. In heat treated unfinished samples, dislocations were able to break the larger precipitates, thus decreasing hardness (Szajewski et al., 2020).

Figure 5 Cutting forces generated, (a) force before applying ultrasonic vibration, (b) force due to ultrasonic vibration (see online version for colours)

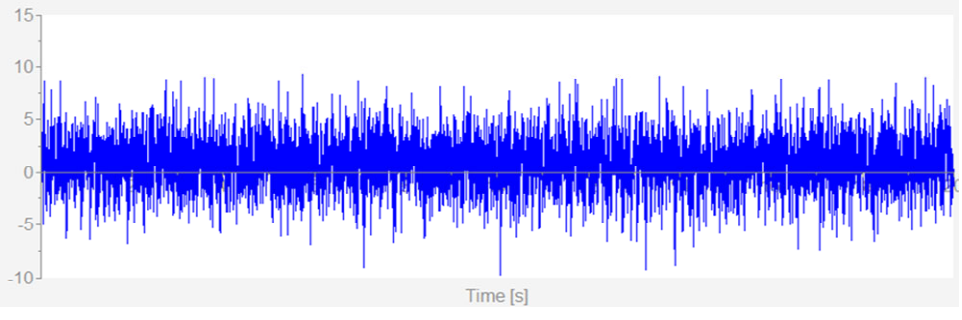

(a)

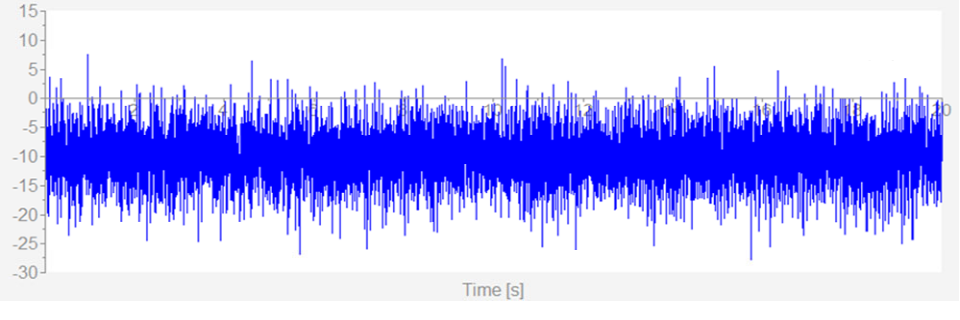

(b)

UAMAF performed on non-heat-treated unfinished sample led to an increase in hardness due to the embedment of abrasive particles in open cavities left on the surface formed because of partially or unbound metal powder particles, evident from Figure 7(a). In heat treated unfinished sample, heat treatment combined with UAMAF reduced surface hardness to some extent. This was due to the hindering of abrasive embedment in surface cavities or pores. Heat treatment reduced cavity size by bounding unbound powder particles. Repeated impact of abrasive particles due to sinusoidal path of abrasives in UAMAF also allowed material flow decreasing surface cavities thus hindering abrasive embedment reducing hardness [Figure 7(c)].

Figure 6 Micro hardness of various SLM built AlSi12Mg samples (see online version for colours)

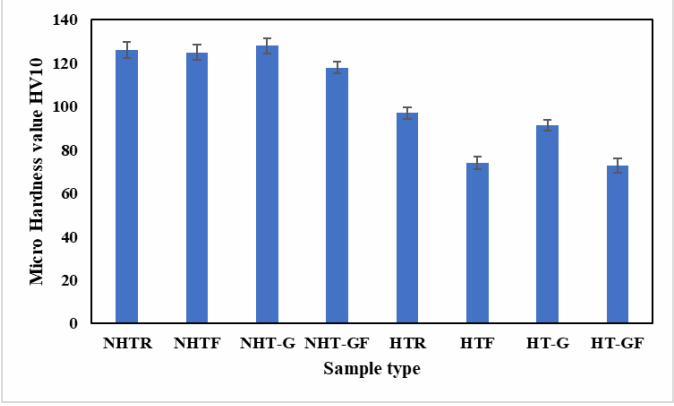

Figure 7 Microstructure, (a) showing abrasives embedded into the pores of NHT sample, (b) grinded finished heat-treated sample (HT-GF), (c) abrasive flow direction (see online version for colours)

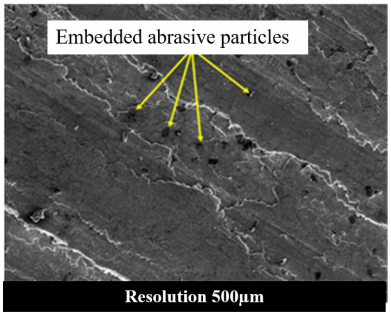

(a)

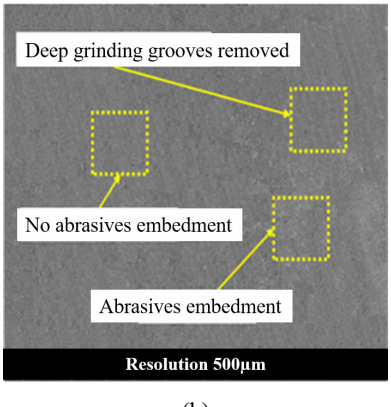

(b)

Figure 7 Microstructure, (a) showing abrasives embedded into the pores of NHT sample, (b) grinded finished heat-treated sample (HT-GF), (c) abrasive flow direction (continued) (see online version for colours)

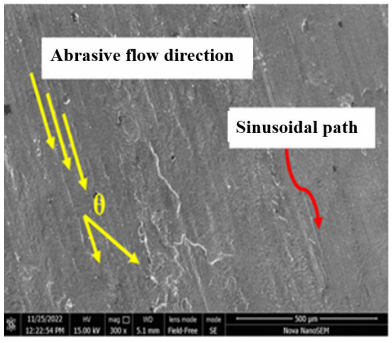

(c)

Figure 8 Forces during UAMAF (see online version for colours)

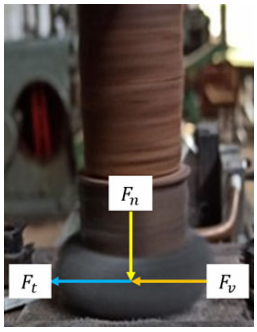

Grinding of heat treated unfinished and non-heat-treated unfinished samples led to increase in surface hardness due to work hardening effect because of heat generation and immediate cooling during the grinding process. UAMAF performed on ground samples relieved hardness due to repeated abrasive impacts caused due to three forces [thrust force by iron particles in magnetic lines (F_n), tangential force by rotation of electromagnet (F_t), linear force by ultrasonic vibrations (F_v)] (Figure 8). The thrust force (F_n) helps in holding the abrasives not to escape from FMAB. As the thrust is increased by increasing the voltage, the rigidity of the FMAB increases and UAMAF finishing efficacy increases. The tangential force (F_t) increases due to rise in rotational speed of electromagnet, which improves the abrasives hitting force on the surface asperity and reduces the finishing time. F_v generated by perpendicular vibrations increases the number of active abrasive particles and decreases the finishing time. From the above discussions, initial hardness of non-heat-treated unfinished sample was very high due to Si chain network and its hardness rapidly increased during grinding process due to work hardening effect (Cui et al., 2022). UAMAF is more effective in decreasing surface hardness in case of heat-treated sample which is due to low initial hardness by heat treatment. Though grinding increased the hardness comparatively, considering the initial hardness, even after UAMAF heat treatment, the sample possessed low hardness due to relieving of hardness by abrasive impacts.

3.2 Wear analysis

Figure 9 shows a bar graph for mass loss in various samples. Mass loss for non-heat-treated unfinished sample was lower compared to heat treated unfinished sample. As mass loss of the material depends on surface roughness, non-heat-treated unfinished sample possessed higher surface roughness compared to heat treated unfinished sample shown in Figure 10. This is due to high surface roughness which indicates more sharp peaks; these peaks possess high stress concentration. When a perpendicular load acts on these peaks, material reaches failure point and breaks due to sliding friction. In contrast to this, non-heat-treated unfinished sample is prone to lower mass loss due to high hardness, which is due to finer grain structure. Heat treated unfinished sample on the other side softened due to heat treatment and Si network breakage which caused a decrease in hardness. The decrease in hardness caused more mass loss though it possesses lower surface roughness. Initial wear was due to high surface roughness in both samples. As initial surface roughness was high in non-heat-treated unfinished sample, the mass loss was more in such a sample.

Figure 9 Bar graph showing mass loss in grams vs. sample type (see online version for colours)

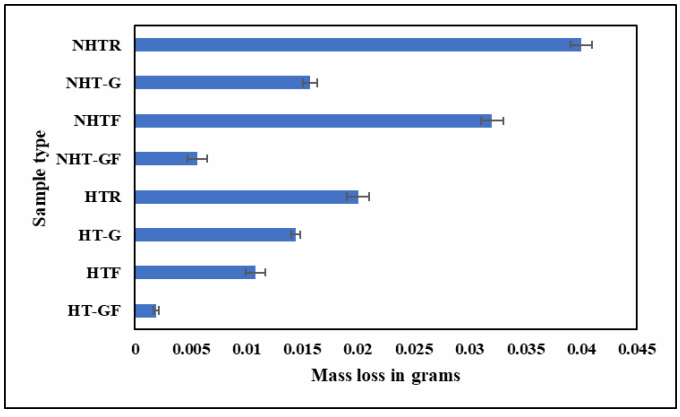

UAMAF on non-heat-treated unfinished sample led to slight improvement in surface finish which was due to rapid abrasive impact resulting from sinusoidal path of abrasives break peaks. Mass loss in non-heat-treated finished sample was lower compared to non-heat-treated unfinished sample, which was due to reduction in sharp peaks after UAMAF. Mass loss in non-heat-treated grinded sample was lower compared to both non-heat treated unfinished and non-heat-treated finished samples. Grinding process effectively decreased initial surface roughness (Figure 10) to some extent, thereby decreasing wear so that mass loss was low. UAMAF performed on the ground sample drastically decreased surface roughness and this decreased mass loss. Rapid impact of abrasives on the sample in UAMAF processed non-heat-treated grinded sample surface better compared to non-heat-treated unfinished sample as the grinding process reduced high surface peaks initially present on the surface. Thus, mass loss was lower in non-heat treated grinded finished sample compared to all samples of non-heat-treated type.

Based on Archard's equation, mass loss of a material is inversely proportional to its hardness under adhesive wear conditions (Kauzlarich and Williams, 2001). Post heat treatment resulted in improvement of initial wear and frictional characteristics. The

decrease in initial wear was due to the remelting of unbonded or partially sintered powder particles that resulted in a decrease in surface peaks. Heat treated unfinished sample is prone to low initial wear but a decrease in hardness caused extra wear. UAMAF on it decreased mass loss to some extent due to reduction in surface peaks through rapid abrasive impact. Mass loss in heat treated grinded finished sample was lowest of all samples discussed, which was due to strain hardening in ground samples made wear resistant, and this decreased mass loss. So initial wear due to peaks and secondary wear due to softening of material caused by heat treatment was avoided in heat treated samples decreasing mass loss.

3.3 Corrosion analysis

The slope of Tafel plots [Figures 11(a) and 11(b)] was used to calculate i_{corr} values (Table 4). In non-heat-treated unfinished sample, the presence of continuous eutectic silicon network in the sample caused a small driving force for corrosion [Figure 13(a)]. Post heat treatment caused breakage of Si chains, forming large, isolated, and uniformly distributed silicon particles, which increased the driving force for corrosion [Figure 13(b)]. So, non-heat-treated unfinished sample is more corrosion resistant compared to heat treated unfinished sample initially.

Figure 10 R_a vs. sample type (see online version for colours)

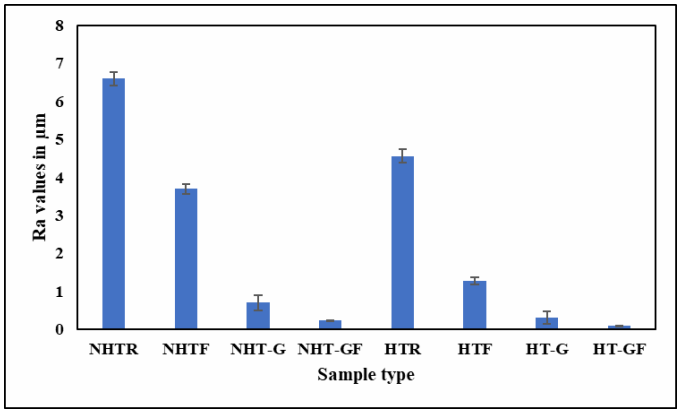

Table 4 Showing type of sample, corrosion current, and corrosion potential

Sample type	*HT-GF*	*NHT-GF*	*HTF*	*NHTF*	*HT-G*	*NHT-G*	*HTR*	*NHTR*
i_{corr} (µA)	0.184	0.231	0.680	1.320	1.570	1.590	4.270	2.671
E_{corr} (mV)	–592.0	–677.0	–703.0	–697.0	–671.0	–645.0	-672.0	–684.0

But surface defects like cavities, high surface roughness, etc. which are present while manufacturing the samples using SLM in both non-heat treated unfinished and heat-treated unfinished samples, significantly increased corrosion rate. The deep valleys in these samples acted as micro-reactive sites which favoured a corrosion environment. These trapped the corrosion media within the valleys and promoted continuous pitting due to corrosion. The rough surfaces in these samples shared more interfacial area with the corrosive environment which in turn enhanced corrosion, which is evident from

Figure 11. The intersection point of cathodic and anodic curves in Tafel plots is shown in Figure 11. The shift of this intersection point towards the positive side makes it more corrosion resistant.

Figure 11 Overlay of Tafel polarisation curves, (a) NHT samples, (b) HT samples (see online version for colours)

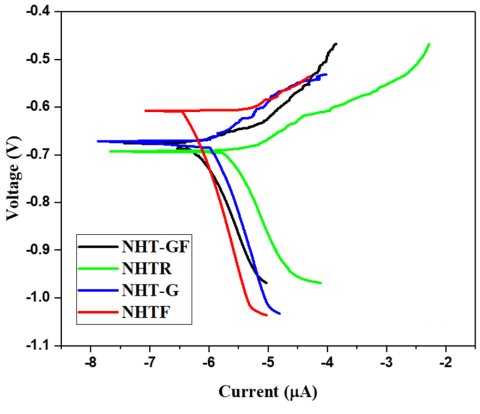

(a)

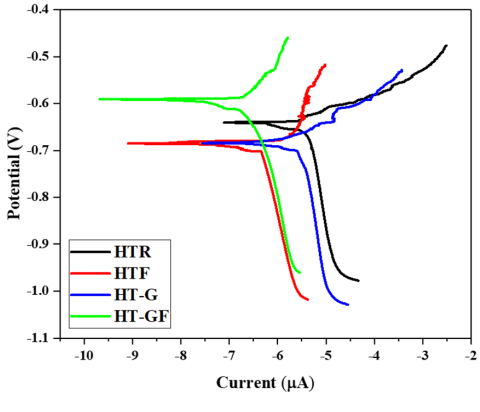

(b)

Initial surface roughness played a critical role on the finishing efficiency of UAMAF. When initial surface roughness was high, there was a decrease in finishing efficiency of UAMAF in both heat-treated unfinished and non-heat-treated unfinished samples. As the initial surface roughness was high in SLM samples, no effective finishing occurred and thus high surface roughness enhanced corrosion rate. From equation (1), it can be interpreted that corrosion rate totally depends on corrosion current (i_{corr}). The i_{corr} values of various samples are mentioned in Table 4 and a comparison is shown in Figure 12. Thus, heat treated unfinished sample is more prone to corrosion as its i_{corr} is 4.270 μA which is highest among all samples. This was due to eutectic Si network which showed more corrosion. Heat treatment enhanced surface quality due to remelting of surface material thus decreasing corrosion sites, but Si network breakage caused increased

corrosion rate. So, the corrosion rate of heat-treated unfinished sample was more compared to non-heat-treated unfinished sample.

Figure 12 Bar graph showing material type and there i_{corr} values (see online version for colours)

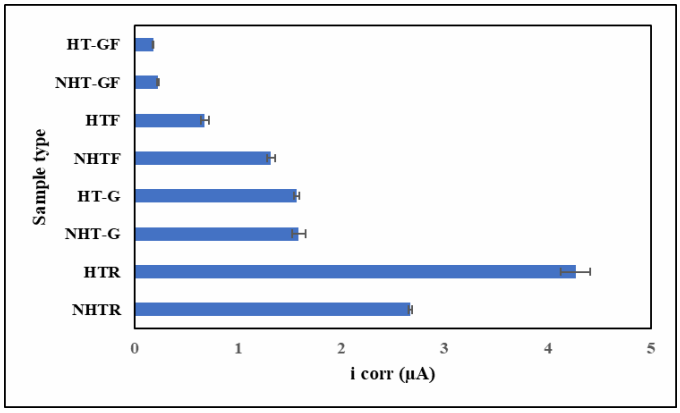

Grinding produced deep groves on the surface and these grooves acted as corrosion sites and corrosive media settled in the valleys for more time. But grinding process effectively finished most of the large size peaks thereby decreasing corrosion spots. Thus i_{corr} values after grinding were 1.59 and 1.57 µA in non-heat treated grinded and heat-treated grinded samples respectively and these values were lower compared to heat treated unfinished and non-heat-treated unfinished samples. UAMAF applied on ground samples made the surface finish better by removing grinding grooves, thereby reducing corrosion sites and by extension corrosion rate as well. Thus the i_{corr} values were very low in non-heat-treated ground, processed and heat-treated ground finished samples, as shown in Table 4. UAMAF combined with grinding effectively decreased the majority of surface peaks, thus decreasing corrosion spots in case of both heat treated and non-heat-treated samples. Comparatively, considering surface finish and corrosion behaviour, the heat-treated sample was better compared to non-heat-treated sample. Heat treatment combined with grinding process and UAMAF resulted in a reduction in corrosion rate.

Although the printed alloy had a little advantage, the corrosion resistance of the cast and printed alloys was comparatively similar. The printed alloy's corrosion fatigue endurance was somewhat better than the cast alloys (Leon et al., 2016; Pant et al., 2022). This was mostly owing to notable variations in microstructure and defect characteristics between the two alloys. Particularly, in the presence of chloride, the surface roughness may increase the alloys' natural sensitivity to localised corrosion attack. The cast alloy had a consistent dendritic microstructure with precipitants that were concentrated in Fe-Mn and Si's eutectic phase. The cast alloy also has usual porosity flaws that come with regular casting procedures by nature. The corrosion attack in cast alloy was much more intense, with an overlap of early corrosion sites and consequently higher corrosion products, whereas the localised corrosion attack in the printed alloy was relatively more dispersed. Due to the micro galvanic impact, the corrosion attack on cast alloy had ideally occurred at the casting flaws and adjacent to Fe-Mn enriched precipitates. It was observed in the printed alloy that corrosion attack tended to advance along the melt pool overlap that had porosity as a built-in feature of the SLM process. When compared to

printed alloy, the breaking started from surface pitting and spread across the sample, generating a comparatively smooth fracture surface before finally snapping.

Figure 13 Microstructure of SLM printed AlSi12Mg: (a) initially solidified Al rich phase (dark) and eutectic Si particles (bright), (b) Al network has been broken and coarse Si particles were formed after HT (see online version for colours)

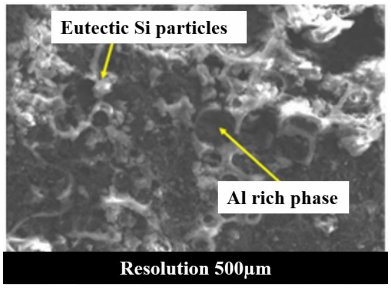

(a)

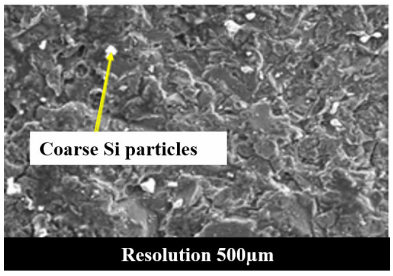

(b)

In the instance of cast alloy, it was clear that cracking began from a crooked defect that was extremely close to the surface area, and the crack spread across the sample primarily along the casting flaws. Several factors can account for the cast alloy's comparatively low corrosion resistance. This understanding suggests that several factors can account for the cast alloy's comparatively poor corrosion resistance.

1 the existence of inherent casting flaws, most notably irregular porosity

2 the relatively intensive formation of enriched Fe and Mn precipitates (MnFe4Al12Si2) that have a negative micro galvanic effect

3 the dendritic microstructure with a secondary eutectic phase that restricts the alloy's ability to dissolve and homogeneity.

The enhanced solidification rate achieved by the SLM method, on the other hand, is primarily responsible for the relative better corrosion resistance of the printed alloy. With enhanced dissolving of alloying elements and impurities and almost no precipitates, this has led to the development of a considerably more homogeneous microstructure. Corrosion resistance is known to improve overall by this microstructure. When opposed to a cast counter material with a dendritic microstructure, the fundamental benefit of aluminium alloys produced through AM is higher mechanical and formability capabilities because of the refined grain structure (due to very high solidification rate).

4 Conclusions

In the present work, sample building was performed on SLM machine and to understand the influence of heat treatment on surface characteristics of samples, the samples were divided into heat treated and non-heat-treated categories. UAMAF on as-built, grinding process combined with UAMAF was performed and tests like corrosion analysis, micro hardness, and wear tests were carried out and the conclusions are as follows:

- Initial surface roughness was the parameter that impacted the finishing efficiency of UAMAF. Low cutting forces in UAMAF cannot remove the large size peaks and even they able to remove the peaks it takes more time thus finishing time increases.
- Elemental composition was almost stable even after UAMAF was done on both heat-treated and non-heat-treated samples. Microstructural studies revealed that a great number of abrasives embedded in pores of non-heat-treated unfinished samples increased surface hardness, thus reducing mass loss.
- Heat treatment reduced micro hardness due to Si precipitation and grain refinement; UAMAF combined with grinding process helped in achieving the desired hardness and surface finish. There was 63.49% and 24.94% drop in hardness in non-heat treated and heat-treated samples respectively. Rapid cooling effect in SLM caused high hardness in non-heat-treated samples because of which UAMAF was not that effective in the case of these samples.
- Mass loss was 0.0019 and 0.0056 g in heat treated and non-heat-treated samples, mass loss was 66.07% lower in heat treated samples. This was due to low initial wear in heat treated sample and the strain hardening that developed in the sample at the time of grinding. UAMAF performed on this sample cannot remove asperities due to high hardness.
- Corrosion rate improvement was 91.35% in non-heat-treated samples and 95.69% in heat treated samples because of performing UAMAF combined with grinding process. This may be due to decrease in surface peaks and valleys thus reducing corrosion media resting sites.

Data availability

Data supporting the findings of this study are made available upon reasonable request from the corresponding author.

References

Aboulkhair, N.T., Simonelli, M., Parry, L., Ashcroft, I., Tuck, C. and Hague, R. (2019) '3D printing of aluminium alloys: additive manufacturing of aluminium alloys using selective laser melting', *Prog. Mater. Sci.*, August 2018, Vol. 106, p.100578, DOI: 10.1016/j.pmatsci.2019.100578.

Anjaneyulu, K. and Venkatesh, G. (2023) 'Experimental investigation of finishing forces on Hastelloy C-276 using UAMAF process', *Int. J. Interact. Des. Manuf.*, Vol. 17, No. 2, pp.703–715, DOI: 10.1007/s12008-022-01113-7.

Anjaneyulu, K., Prakash, G. and Venkatesh, G. (2023) 'Modelling of finishing forces on hastelloy C-276 using ultrasonic assisted magnetic abrasive finishing process', *Int. J. Interact. Des. Manuf.*, DOI: 10.1007/s12008-023-01210-1.

Cui, Y. et al. (2022) 'Study on magnetic abrasive finishing process of AlSi10Mg alloy curved surface formed by selective laser melting', *Int. J. Adv. Manuf. Technol.*, Vol. 118, Nos. 9–10, pp.3315–3330, DOI: 10.1007/s00170-021-08138-4.

Dixit, U.S., Pandey, P.M. and Verma, G.C. (2019) 'Ultrasonic-assisted machining processes: a review', *Int. J. Mechatronics Manuf. Syst.*, Vol. 12, Nos. 3–4, pp.227–254, DOI: 10.1504/IJMMS.2019.103479.

Frazier, W.E. (2014) 'Metal additive manufacturing : a review', *Journal of Materials Engineering and Performance*, June, Vol. 23, pp.1917–1928, DOI: 10.1007/s11665-014-0958-z.

Gite, R.E. and Wakchaure, V.D. (2023) 'A review on process parameters, microstructure and mechanical properties of additively manufactured AlSi10Mg alloy', *Mater. Today Proc.*, Vol. 72, pp.966–986, DOI: 10.1016/j.matpr.2022.09.100.

Javidani, M. and Larouche, D. (2014) 'Application of cast Al-Si alloys in internal combustion engine components', *Int. Mater. Rev.*, Vol. 59, No. 3, pp.132–158, DOI: 10.1179/1743280413Y.0000000027.

Jayswal, S.C., Jain, V.K. and Dixit, P.M. (2005) 'Modeling and simulation of magnetic a brasive finishing process', *Int. J. Adv. Manuf. Technol.*, Vol. 26, Nos. 5–6, pp.477–490, DOI: 10.1007/s00170-004-2180-x.

Kauzlarich, J.J. and Williams, J.A. (2001) 'Archard wear and component geometry', *Proc. Inst. Mech. Eng. Part JJ. Eng. Tribol*., Vol. 215, No. 4, pp.387–398, DOI: 10.1243/1350650011543628.

Kottuparambil, R.R., Bontha, S. and Rangarasaiah, R.M. (2018) 'Effect of zinc and rare-earth element addition on mechanical, corrosion, and biological properties of magnesium', *Journal of Materials Research*, pp.1–13, DOI: 10.1557/jmr.2018.311.

Leon, A., Shirizly, A. and Aghion, E. (2016) 'Corrosion behavior of AlSi10Mg alloy produced by additive manufacturing (AM) vs. its counterpart gravity cast alloy', *Metals (Basel)*, Vol. 6, No. 7, DOI: 10.3390/met6070148.

Majeed, A., Ahmed, A., Salam, A. and Zakir, M. (2019) 'Surface quality improvement by parameters analysis, optimization and heat treatment of AlSi10Mg parts manufactured by SLM additive manufacturing', *Int. J. Light. Mater. Manuf.*, Vol. 2, No. 4, pp.288–295, DOI: 10.1016/j.ijlmm.2019.08.001.

Misra, A., Pandey, P.M., Dixit, U.S., Roy, A. and Silberschmidt, V.V. (2019) 'Multi-objective optimization of ultrasonic-assisted magnetic abrasive finishing process', *Int. J. Adv. Manuf. Technol.*, Vol. 101, Nos. 5–8, pp.1661–1670, DOI: 10.1007/s00170-018-3060-0.

Pant, M., Nagdeve, L., Moona, G., Kumar, H. and Sharma, A. (2022) 'Tribological behavior investigation of 316L stainless steel samples processed by selective laser melting', *Proc. Inst. Mech. Eng. Part J. J. Eng. Tribol.*, Vol. 237, No. 4, pp.718–731, DOI: 10.1177/13506501221101797.

Raju, T.B. and Hithaish, D. (2014) 'Additive Manufacturing in Automobile Industry', *International Journal of Research in Aeronautical and Mechanical Engineering*, Vol. 2, No. 3, pp.224–231.

Shiyas, K.A. and Ramanujam, R. (2021) 'A review on post processing techniques of additively manufactured metal parts for improving the material properties', *Mater. Today Proc.*, Vol. 46, pp.1429–1436, DOI: 10.1016/j.matpr.2021.03.016.

Singh, D.K., Jain, V.K. and Raghuram, V. (2006) 'Experimental investigations into forces acting during a magnetic abrasive finishing process', *Int. J. Adv. Manuf. Technol.*, Vol. 30, Nos. 7–8, pp.652–662, DOI: 10.1007/s00170-005-0118-6.

Singhal, T.S. et al. (2023) 'A comprehensive comparative review: welding and additive manufacturing', *Int. J. Interact. Des. Manuf.*, DOI: 10.1007/s12008-022-01152-0.

Spears, T.G. and Gold, S.A. (2016) 'In-process sensing in selective laser melting (SLM) additive manufacturing', *Integrating Materials and Manufacturing Innovation*, DOI: 10.1186/s40192-016-0045-4.

Suniya, N.K. and Verma, A.K. (2023) 'A review on optimization of process parameters of fused deposition modeling', *Research on Engineering Structures and Materials*, Vol. 9, No. 2, DOI: 10.17515/resm2022.520ma0909.

Szajewski, B.A., Crone, J.C. and Knap, J. (2020) 'Analytic model for the Orowan dislocation-precipitate bypass mechanism', *Materialia*, March, Vol. 11, DOI: 10.1016/j.mtla.2020.100671.

Tawalbeh, M., Khan, H.A., Al-Othman, A., Almomani, F. and Ajith, S. (2023) 'A comprehensive review on the recent advances in materials for thermal energy storage applications', *Int. J. Thermofluids*, March, Vol. 18, p.100326, DOI: 10.1016/j.ijft.2023.100326.

Wong, K.V. and Hernandez, A. (2012) 'A review of additive manufacturing', *ISRN Mech. Eng.*, Vol. 2012, pp.1–10, DOI: 10.5402/2012/208760.

Wu, P.Y. and Yamaguchi, H. (2018) 'Material removal mechanism of additively manufactured components finished using magnetic abrasive finishing', *Procedia Manuf.*, Vol. 26, pp.394–402, DOI: 10.1016/j.promfg.2018.07.047.

Yamaguchi, H., Srivastava, A.K., Tan, M.A., Riveros, R.E. and Hashimoto, F. (2012) 'Magnetic abrasive finishing of cutting tools for machining of titanium alloys', *CIRP Annals – Manufacturing Technology*, Vol. 61, No. 1, pp.311–314, DOI: 10.1016/j.cirp.2012.03.066.

Yousefzadeh, S. and Safari, M. (2012) 'An analysis of curved tubes finishing by magnetic abrasive finishing', *Int. J. Surf. Sci. Eng.*, Vol. 6, Nos. 1–2, pp.81–91, DOI: 10.1504/IJSURFSE.2012.046844.

Zhang, B. et al. (2022) 'Effect of heat treatment on the microstructure and mechanical properties of Er-containing Al-7Si-0.6 Mg alloy by laser powder bed fusion', *J. Mater. Res. Technol.*, Vol. 18, pp.3073–3084, DOI: 10.1016/j.jmrt.2022.04.023.

Zhang, J., Chaudhari, A. and Wang, H. (2019) 'Surface quality and material removal in magnetic abrasive fi nishing of selective laser melted 316L stainless steel', *J. Manuf. Process.*, August, Vol. 45, pp.710–719, DOI: 10.1016/j.jmapro.2019.07.044.

Zhu, P. et al. (2022) 'Investigation and process optimization for magnetic abrasive finishing additive manufacturing samples with different forming angles', *Int. J. Adv. Manuf. Technol.*, Vol. 118, No. 7–8, pp.2355–2371, DOI: 10.1007/s00170-021-08083-2.

Abbreviations

NHTR	non-heat treated as-built
NHT-G	non-heat-treated grinded (post grinding process)
NHTF	non-heat treated finished (post UAMAF)
NHT-GF	non-heat treated grinded finished (post grinding process and UAMAF)
HTR	heat treated unfinished (post heat treatment)
HT-G	heat treated grinded (post grinding process)
HTF	heat treated finished (post UAMAF)
HT-GF	heat treated grinded finished (post grinding process and UAMAF).